Presented at the UGV Technology Conference at the 2002 SPIE AeroSense Symposium, Orlando, FL, April , 1-5, 2002

Experimental Characterization of Polaroid Ultrasonic Sensors in Single and Phased Array Configuration

Alex Cao* and Johann Borenstein**

The University of Michigan, Department of Mechanical Engineering

ABSTRACT

Many mobile robots use Polaroid ultrasonic sensors for obstacle avoidance. This paper describes the experimental characterization of these sensors using a unique, fully automated testbed system. Using this testbed, we gathered large data sets of 5,000-16,000 data points in every experiment for characterization purposes; in a repeatably fashion and without human supervision.

In the experimental characterization reported in this paper we focused on a comparison of the "beamwidth" of a single sonar with that of a dual sonar phased array. For the single sonar we found that flat walls trigger echo signals up to an angle of ±42º, which is well beyond the traditional assumed beamwidth of ±15º. We determined that these echoes result from the secondary and tertiary lobe of the well known multi-lobed propagation patterns of Polaroid ultrasonic sensors. In contrast, with the dual sonar phased array echo signals were triggered only up to beamwidths of ±18º. By implementing a power-reducing modification in the sonar circuits, we achieved narrow beamwidths of 4-6°. The results in this paper were obtained for two test targets: a specular surface and a cylindrical object.

1. INTRODUCTION

Polaroid ultrasonic sensors (interchangeably referred to as "sonars" in this paper), have a relatively wide wave propagation profile (for simplicity called "beamwidth" in this paper) estimated in most of the mobile robotics-literature to be about ±15º. This wide beamwidth is undesirable in most mobile robot application because it obscures the dimensions of obstacles, making it very difficult to navigate through narrow openings like doorways.

Indeed, as our experiments show, for many obstacles configurations echoes are still detectable even if the sonar "beam" hits the target at an incident angle of more than the somewhat arbitrarily defined ±15º. The purpose of this paper is to present very detailed experimental results on the effective beamwidth of the Polaroid sonars, and results of our attempts to narrow the beamwidth using a variant of so-called phased arrays. Section 2 discusses in more detail the relevant characteristics of the Polaroid sonar and compares our dual-sonar approach to other phased array approaches described in the literature. Section 3 describes in some detail the test environment and our unique sensor testbed that enabled us to conduct the data rich experiments described in Section 4.

2. THE ULTRASONIC SENSORS

The ultrasonic sensors used in our experiments was the Polaroid 6500 Series (see Figure 1), which is commonly used on mobile robots for obstacle avoidance. This sonar operates at its resonance frequency of 50 kHz. One key

* caoa@engin.umich.edu, phone 734-936-9362; University of Michigan, Advanced Technologies Lab, 1101 Beal Ave., Ann Arbor, MI 48109-2110. **Corresponding author: johannb@umich.edu, phone 734-763-1560; fax: 209-879-5169; University of Michigan, Advanced Technologies Lab, 1101 Beal Ave., Ann Arbor, MI 48109-2110.

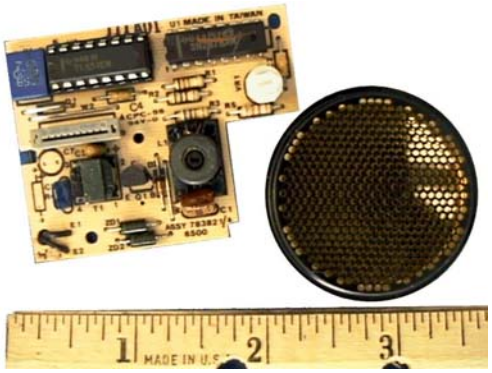

Figure 1: The Polaroid 6500 Series ultrasonic sensor used in our experiments.

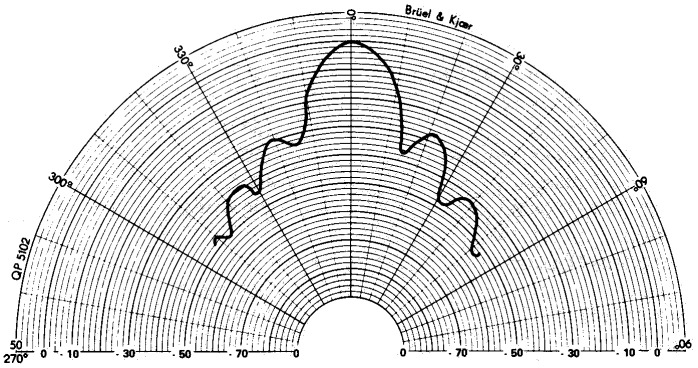

Figure 2: Typical propagation pattern for the Polaroid 6500 Series ultrasonic sensor. Courtesy of Polaroid [1].

characteristic of ultrasonic sensors is the propagation pattern, also illustratively called "beamwidth" in this paper. The propagation pattern for the Polaroid 6500 sensor is shown in Figure 2. We will define "lobes" as the angular range between the normal direction, i.e., 0°, and a zero of the first derivative of the plot. As can be seen in Figure 2, the primary lobe is about ±15º wide. The secondary lobe is about ±30º and the tertiary lobe is about ±45º wide. Another angle of interest is the one related to the –3 dB point, but we will not considered this point in our discussion.

In most mobile robot obstacle avoidance systems ultrasonic sensor data is not directly reacted upon. Rather, the data is used to build or augment a real-time map of the environment. For this map-building task a large beamwidth is undesirable since it increases the uncertainty about the actual location of an obstacle. The result of this uncertainty is that obstacles tend to be represented in the map as larger than they really are, which, in turn, leads mobile robots to avoid narrow openings even though the opening might be passable.

One method aimed at reducing the effective beamwidth of sonars is based on so-called "phased arrays." Phased arrays are well known as a means for changing the radiation pattern of transducers through their mutual constructive and destructive interferences. They are used in many applications such as radar, sonar, and medical ultrasound. These applications often involve a large number of array elements usually numbering in the hundreds. Several techniques have been developed to eliminate or suppress side lobes from these arrays. Moshfeghi [2] investigated the use of different size apertures on the transmitter and receiver. Cincotti [3] performed aperture windowing by controlling the length of the electric pulse driving the array elements. Others use complex weight vectors with retrodirective beams and computational schemes to eliminate all grating lobes [4, 5]. Grating lobes are defined as the lobes beyond the primary lobe such as secondary and tertiary lobe. The improvements in sidelobe response are generally obtained at the expense of a widening of the primary lobe. Other approaches include using physical constraints in the form of a cylindrical waveguides to create a narrow acoustic beam [6]. Optimization techniques of the beam pattern for unequally spaced arrays [7] and for 1-D and 2-D sparse arrays [8, 9] have also been developed.

Less work has been reported on airborne ultrasound for obstacle avoidance. The University of Nottingham developed and manufactured custom airborne ultrasonic arrays on a printed circuit board operating at 100 kHz [10, 11]. The whole board is used as a transmitter while small segments on the board can act as individual receivers. They were able to construct their array with the desired sub λ/2 element spacing and used this array for robot guidance [12] using a beam-forming technique. They were able to increase the element spacing above the λ/2 limitation to 11λ through new processing methods [13] while working on reducing the computational effort [14]. Kleeman and Kuc [15] presented a sonar configuration and processing approach that can accurately classify and localize planes, corners, and edges without sensor movement using two transmitters and receivers.

In our work reported here, we aimed at producing a simple phased array that would still provide the desired narrower beamwidth (when compared to a single sonar). We wanted to use the off-the-shelf Polaroid hardware without significant modifications. Another desirable property was minimal computational time to allow our algorithms to be implemented on mobile robots with limited on-board computing power.

Acoustic field theory [16, 17] is able to predict radiation patterns for a variety of phase arrays configurations. For example, the nulls in the radiation pattern of a line array are given by:

$$\left|\sin\theta_n\right| = \frac{n}{N}\frac{\lambda}{d} \tag{1}$$

where N is the number of elements, λ is the wavelength, and d is the element spacing. The first null in the beam pattern corresponds to $n = 1$. In air at room temperature the wavelength of ultrasound is about 6.8 mm.

To avoid grating lobes, an element spacing of less than or equal to $\lambda/2$ is desired. This spacing places the first null at an angle $\geq 90^\circ$ thus eliminating any grating lobes. This is impractical in our case since the transducers are significantly larger than half the wavelength of the signal. Thus we cannot eliminate the grating lobes entirely. As the spacing between transducers increases, the angle at which the first null appears also decreases according to (1). This has the effect of reducing the beamwidth of the primary lobe.

In our experiments we created a simple phased array from two off-the-shelf Polaroid sonars. Mounting one sonar about 50 mm above the other was expected to result in a beamwidth of ±4º, according to Eq. (1). We could have increased the spacing further but there is a tradeoff between the beamwidth of the primary lobe and the peak level of the secondary lobe. This simple phased array is explained in more detail in Section 4.3 . Our use of a phased array with a small number of elements (2) is by no means new, for example, a 4-element phased array was used as early as 1987 on Hermies-IIB at the Oak Ridge National Lab [18].

3. TEST ENVIRONMENT

All experiments described in this paper were conducted using a unique, fully computerized testbed, show in Figure 3. This section describes the testbed in some detail.

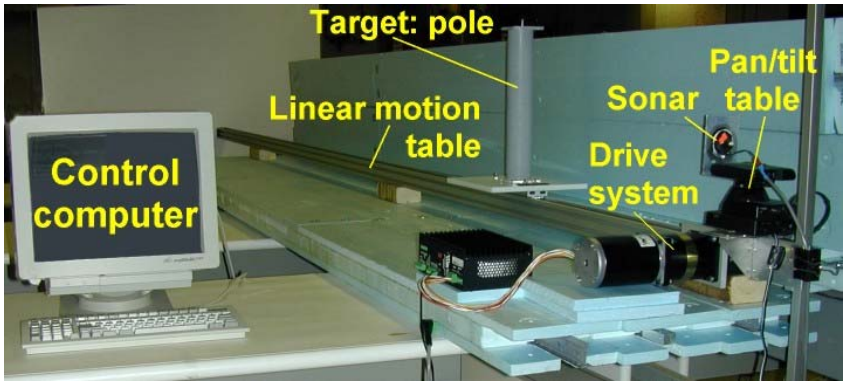

Figure 3: The fully automated test bed uses a 4-meter linear motion table to move the target and a pan/tilt table to orient the sensor.

3.1 The Automated Testbed System

The central element of our automated testbed is a 4-meter long linear motion table [19]. It consists of a carriage on a conveyor belt controlled by a stepper motor with variable resolution. The step size used in the experiments was 0.012 mm/step. The motor has a maximal speed of 1.18 m/s and a maximal acceleration rate of 70 m/s^2. The acceleration is linear thus giving a trapezoidal velocity profile. The table is controlled through the serial port of a PC. The PC can also query the motion table's controller about the momentary position of the carriage. This ability is important for validating sonar readings in real time during motion.

A pan/tilt unit [20] is used to move the sensor. The range of the unit is ±90º in the pan direction and +25º/-30º in the tilt direction. The resolution of the unit is 0.115º. This unit is controlled through the second serial port of the control PC.

A PC-interfaced digital oscilloscope, model ADC200-50 from Pico Technology Limited [21], is used in some of the experiments described below. It has a maximum sample rate of 50 MHz and is controlled via the parallel port of the PC.

The automated testbed system is an effective tool for the large-scale experimental characterization of different sensors. Since it is fully automated, the system can produce characterization results, such as the ones presented in Section 4, without human intervention. The graphs presented in Section 4 represent anywhere between 5,000-16,000

individual data points, collected fully automatically in experiments taking no longer than 2.5 hours. Another advantage of this system is that it offers great repeatability of test conditions and measurements.

3.2 Obstacle Avoidance Targets Used in the Experiments

Two primary targets were used in the sonar tests. The first was a Ø1.75" cardboard tube. The pole represents slender cylinder-type objects commonly found in domestic or urban environments. The second target was a 2×8 ft. (height × width) vertically-mounted plywood board. The board's surface is representative of smooth specular surfaces like walls. Due to practical constraints, the sonar was tested in only one direction with the assumption of symmetric behavior as suggested by the plot in Figure 2. For experiments with the pole, however, the full beamwidth of the sonar was examined.

4. EXPERIMENTAL RESULTS

In this section we provide results from experiments with the single and double sonar configuration. For either set of experiments the procedure was the same, as explained in the next subsection.

4.1 Experimental Procedure

The experimental results presented in this section were all obtained with the same test procedure. Initially the sonar(s) faced 90° to the left. The target was mounted on the motion table's carriage at an initial distance of 500 mm. The control computer then performed the following steps in each experiment, all without human intervention:

1. The carriage moved away from the sonar(s) and range measurements were taken at 25 mm intervals while the target was in motion. The steady-state speed of the target was 0.1 m/sec.
2. Once the target reached a predetermined maximum distance from the sonar(s), the carriage stopped and the sonar range measurements were halted. The maximum distance was 3,000 mm for the board and 3,500 mm for the pole.
3. The target then returned to the initial starting position, i.e., to a distance of 500 mm from the sonar(s), and the sonar(s) were panned (i.e., rotated) 2º toward the forward (0°) direction.
4. Steps 1-3 were repeated until the sonar(s) had swept through 90º (for the board) or 180º (for the pole).

We plotted the results of the experiments as single blue dots on a Cartesian coordinate frame, as seen, for example, in Figure 4. Each single blue dot was plotted at a distance from the origin that corresponded to the range measured by the sonar and in the direction the sonar was facing at the time of measurement. Because of the density of our measurements, consecutive dots appear as solid lines in the resulting plots. The circular arcs in the graphs represent equi-distances from the origin, i.e., the location of the sonar(s).

4.2 Baseline results with a single sonar

A baseline case was first established for both targets, the board and the pole. Results show that echoes were detected within a pan range of up to 42º for the board (Figure 4a) and ±10º for the pole (Figure 4b). For the board, echoes are being received from not only the primary lobe, but also from the secondary and tertiary lobe when

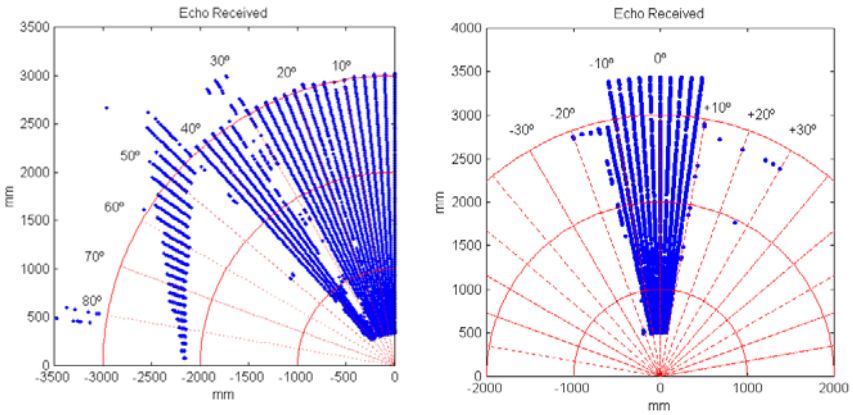

Figure 4: Baseline results for measuring distance to (a) the board and (b) the pole placed at different distances and with the sonar paned to different angles between 0 and 90°.

compared to the Polaroid beam pattern in Figure 2. This is interesting because, as we mentioned in the Introduction, virtually all sonar-based obstacle avoidance algorithms described in the scientific literature assume echoes only from the primary lobe and not from the secondary or tertiary lobes. A smaller detectable beam angle would be desirable to eliminate the uncertainty resulting from wide beam angles, as explained in Section 1.

Another interesting observation can be made from Figure 4a, where the outliers located beyond 42º look as though they were lined up and right-justified. We determined that these echoes were produced by the left-hand edge of the board as it moved away from the sonar(s). We also verified that the line formed by these outliers did indeed correspond to the vertical edge of the board, which, in our experiment moved back and forth in parallel to the linear motion table. For cylindrical objects, such as the pole in our experiments, this is not a problem as echoes are only being received from the primary lobe.

4.3 Dual sonar configuration

In order to characterize the behavior of a phased array we first built a mathematical model of a simple dual sonar configuration, with both sonars placed one above the other at a distance of 50 mm from each other. The propagation pattern resulting from this simulated phased array is shown in Figure 5a. The simulation result reflects visually the behavior predicted by the mathematical model based on Eq. 1. Specifically we expected a beamwidth of ±4º measured between the nulls surrounding the primary lobe. This reduction in beamwidth is seen only in the direction of the plane of the sonar array, while the beamwidth in the perpendicular direction is unchanged.

We then mounted two actual sonars in the same phased array configuration, as shown in Figure 6. However, in order to validate our mathematical model we had to modify the experimental setup described in Section 4.1 . This time, instead of mounting a target, we mounted another ultrasonic transducer on the motion table's carriage. Using this transducer as a microphone only, we fed the amplified analog signal from that transducer into a digital oscilloscope. The transducer was placed at a fixed distance of 1,500 mm and the sonars were swept through a range of ±20º in 1º increments through pan and tilt motions. The results are shown in Figure 5b. The experimental results of Figure 5b agree closely with the beam pattern predicted in the numerical simulations of Figure 5a. The symmetry in Figure 5a is due to the simulation assuming the sonars are identical when that is not exactly true in practice as seen in Figure 6b.

After verifying the correspondence between our simulation model and the experimental results, we proceeded to characterize the vertical dual sonar arrangement experimentally and in the fashion described in Section 4.2. The results for the vertical dual sonar are shown in Figure 7. It can be seen that the beamwidth is about 18º, with a few outliers.

Having available range readings from two sonars and the distance of the carriage as measured by the linear motion controller (the "ultimate truth reference," in our experiments), we examined how well these three measurements, which should ideally all be identical, really matched. The results of this examination are shown in Figure 8.

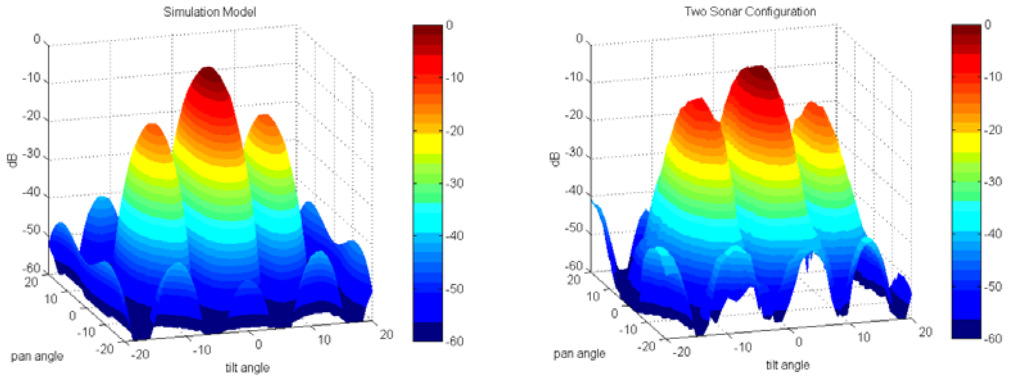

Figure 5: A phased array made of two vertically stacked sonars provides a significantly narrower beam width. (a) Simulation results. (b) Actual experimental results.

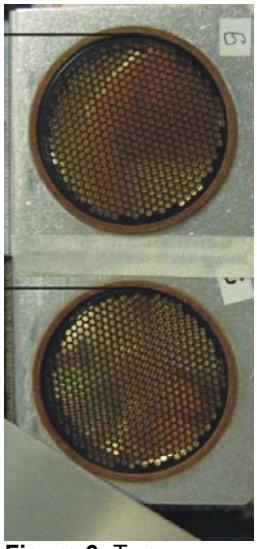

Figure 6: Two vertically stacked sonars form a simple phased array.

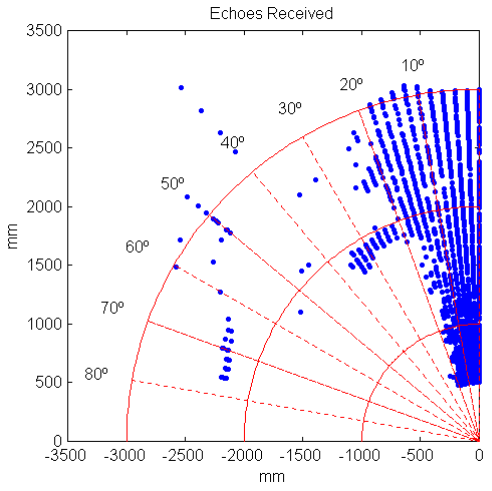

Figure 7: Results for the vertical dual sonar configuration. A beamwidth of 18º is present with a few outliers.

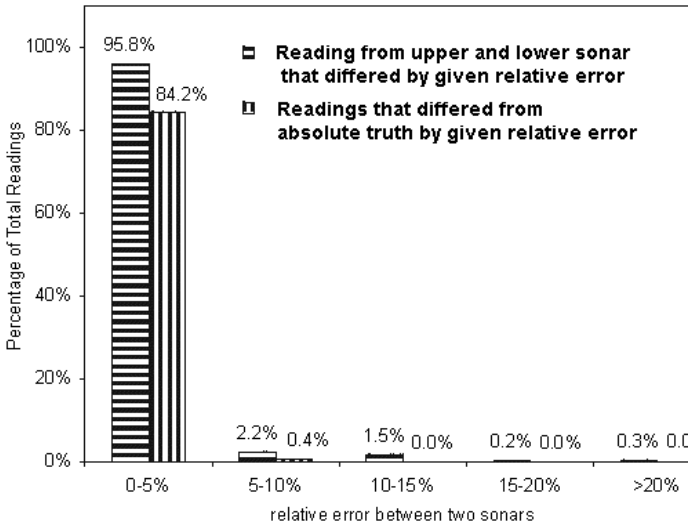

Figure 8: The histogram on the left with the horizontal stripes shows the percentage of readings from the dual sonar configuration that agree within a given relative error range. The histogram on the right with the vertical stripes represents the percentage of readings that are indeed accurate, as verified by the actual distance of the carriage measured by the motion table.

Figure 8 shows this match in histogram form. For example, if readings from the two sonars matched within a relative error of less than 5% (i.e., $|R_1-R_2|/R_1 < 0.05$, where R_1 and R_2 are the readings of the upper and lower sonar, respectively), then that reading belonged to the bin labeled 0-5%. As Figure 8 shows 95.8% of all dual sonar readings fell into this bin, as shown by the horizontally striped bar in Figure 8. We will call the readings belonging to the 0-5% error bin "good" readings. We then compared each good reading with the "ultimate truth reference," and found that 84.2% of all good readings were wrong by less than 5%. We thus concluded that if the readings from the two sonars matched to within a relative error of less than 5%, those readings were also highly likely (i.e., with a certainty of 84.2%) to be accurate. The benefits of the second sonar are therefore two-fold: it implements the phased array, thus reducing the beamwidth, and it can provide a validity check.

4.4 Power considerations

Our numerical simulations for the phased array system predicted an effective beamwidth of ±4 degrees, yet the experimental results of Figure 8 show an effective beamwidth of ±18°. While investigating this discrepancy we concluded that echoes were still being received from the secondary and tertiary lobes of the dual sonar configuration, although the lobes are located closer together because of the phased array design. We further concluded that the unexpectedly strong echoes from the secondary and tertiary lobes were the result of the greater power content of the combined wavefronts from the two vertically stacked sensors.

To correct this problem we attempted to reduce the peak power output of the dual sonar configuration to the peak power output of a single sonar configuration. We reasoned that this would be equivalent to lowering the power content of the secondary and tertiary lobes below the echo detection threshold. We achieve the desired low power configuration by placing 220V Zener diodes in parallel with the existing 400V diodes on the sonar boards. We measured the thus modified power output of the dual sonar configuration and confirmed that it produced the same peak power output as a single sonar.

Our experimental results in Figure 9 show that this configuration produces an effective beamwidth angle of ±6º. The test procedure was slightly altered by panning in increments of 1º instead of 2º to improve angular resolution. The low power configuration manages to reduce the beamwidth by sending out a weaker signal thus lowering the return signal below the echo detection threshold. Results for the pole did not show any significant difference from the experiments without power adjustments and the effective beamwidth was about ±9º.

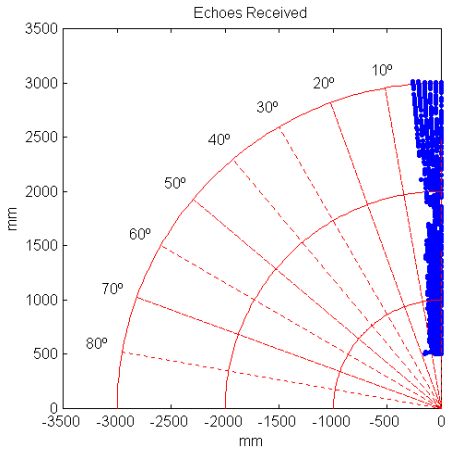

Figure 9: Results for the lower power setting for the dual sonar configuration. A beamwidth of 5º is present with no outliers.

5. CONCLUSION

In this paper we presented detailed results of an experimental characterization of Polaroid ultrasonic sensors. A versatile testbed for the experimental characterization of range measurement sensors was used for this purpose, allowing the fully automated gathering of thousands of range measurements for each experiment.

Our experimental results also show that echoes from vertical walls are triggered for angles of incidence of as much as ±42º, resulting in an undesirably large effective beamwidth. This large beamwidth is the result of so-called secondary and tertiary lobes in the propagation profile of the Polaroid sensors. But, although the existence of these lobes is widely known, few efforts have been made to reduce the effective beamwidth of the Polaroid sonar.

Our paper shows in simulation and actual experimental results that a simple phased array consisting of two vertically stacked sonars can reduce the beamwidth significantly, to about ±6° to ±9°. Furthermore, the dual sonar design not only narrows the effective beamwidth, but also allows for a simple validity check that further reduce the number of misreadings.

Acknowledgement

This work was funded by the U.S. Department of Energy under Award No. DE-FG04-86NE3796.

6. REFERENCES

[1] POLAROID Corp, Ultrasonic Components Group, 119 Windsor Street, Cambridge, MA 02139.

[2] M. Moshfeghi, "Side-lobe Suppression for Ultrasonic Imaging Arrays," *Ultrasonics*, vol. 25, no. 6, Nov. 1987, pp. 322-327.

[3] G. Cincotti et al. "New Beamforming Technique for Ultrasonic Imaging Systems," *Ultrasonics*, vol. 38, no. 1, 2000, pp. 156-160.

[4] P.N. Fletcher and M. Dean, "Application of Retrodirective Beams to Achieve Low Sidelobe Levels in Small Phased Arrays," *Electronics Letters*, vol. 32, no. 6, Mar 14 1996, pp. 506-508.

[5] C.Y. Rew, S.B. Park, J.B. Ra, "Elimination of All Grating Lobes in Ultrasonc Synthetic Focusing using a Linear Array," *Electronics Letters*, vol. 29, no. 19, Sep 17 1993, pp. 1729-1731.

[6] W. Pajewski, P. Kielczynski, M. Szalewski, "Transducers with Narrow Radiation Beam," *Proceedings - IEEE Ultrasonics Symposium*, vol. 2, 1995, pp. 989-992.

[7] J. Lan, R.K. Jeffers, S.G. Boucher, "Optimum Unequally Spaced Arrays and Their Amplitude Shading," *Proceedings - IEEE Ultrasonics Symposium*, vol. 2 1995, pp. 965-969.

[8] A. Austeng et al., "1D and 2D Algorithmically Optimized Sparse Arrays," *Proceedings - IEEE Ultrasonics Symposium*, vol. 2, 1997, pp. 1683-1686.

[9] S. Holm, "Optimization of the Beampattern of 2D Sparse Arrays by Weighting," *IEEE Transactions on Ultrasonics, Ferroelectrics and Frequency Control*, vol. 44, no. 5, Sep 1997, pp. 983-991.

[10] W.S.H. Munro et al. "Ultrasonic Vehicle Guidance Transducer," *Ultrasonics*, vol. 28, no. 6, Nov 1990, pp. 350-354.

[11] W.S.H. Munro and C. Wykes, "Arrays for Airborne 100 kHz Ultrasound," *Ultrasonics*, vol. 32, no. 1, Jan 1994, pp. 57-64.

[12] P. Webb, I. Gibson, C. Wykes, "Robot Guidance Using Ultrasonic Arrays," *Journal of Robotic Systems*, vol. 11, no. 8, Dec 1994, pp. 681-692.

[13] P. Webb and C. Wykes, "High-Resolution Beam Forming for Ultrasonic Arrays," *IEEE Transactions on Robotics and Automation*, vol. 12, no. 1, Feb. 1996, pp. 138-146.

[14] P. Webb and C. Wykes, "Analysis of Fast Accurate Low Ambiguity Beam Forming for Non λ/2 Ultrasonic Arrays," *Ultrasonics*, vol. 39, no. 1, Jan 2001, pp. 69-78.

[15] L. Kleeman and R. Kuc, "Optimal Sonar Array for Target Localization and Classification," *Proceedings - IEEE International Conference on Robotics and Automation*, pt. 4, ,1994, pp. 3130-3135.

[16] L.E. Kinsler et al., *Fundamentals of Acoustics 4th Ed.*, New York: Wiley, 2000.

[17] L.J. Ziomek, *Fundamentals of Acoustic Field Theory and Space-Time Signal Processing*, Boca Raton: CRC Press, 1995.

[18] Burks, B.L. et al., "Autonomous Navigation, Exploration, and Recognition Using the HERMIES-IIB Robot." *IEEE Expert*, Winter 1987, pp. 18-27.

[19] Applied Motion Products, 404 Westridge Dr., Watsonville, CA 95076.

[20] Canon U.S.A., Inc. One Canon Plaza, Lake Success, NY 11042.

[21] Pico Technology Limited, The Mill House, Cambridge Street, St. Neots, PE19 1QB, United Kingdom